Article

Insights into Decomposition Pathways and Fate of Ru(bpy)32+ during Photocatalytic Water Oxidation with S2O82- as Sacrificial Electron Acceptor

Umme Sarmeen Akhtar, Eunju Lee Tae, Yu Sung Chun, In Chul Hwang, and Kyung Byung Yoon

ACS Catal., **Just Accepted Manuscript** • DOI: 10.1021/acscatal.6b02595 • Publication Date (Web): 02 Nov 2016

Insights into Decomposition Pathways and Fate of $Ru(bpy)_3^{2+}$ during Photocatalytic Water Oxidation with $S_2O_8^{2-}$ as Sacrificial Electron Acceptor

*Umme Sarmeen Akhtar,† Eunju Lee Tae, Yu Sung Chun, In Chul Hwang, Kyung Byung Yoon**

Korea Center for Artificial Photosynthesis, Center for Nanomaterials, and Department of Chemistry, Sogang University, Seoul 121-742, Korea. e-mail: yoonkb@sogang.ac.kr

ABSTRACT: The most widely accepted system for homogeneous photocatalytic water oxidation process consists of a water oxidation catalyst, $Ru^{II}(bpy)_3^{2+}$ as a photopump, and $S_2O_8^{2-}$ as the sacrificial electron acceptor. However, this system is far less than ideal because $Ru^{II}(bpy)_3^{2+}$ undergoes very rapid decomposition and as a result the process stops before all of $S_2O_8^{2-}$ is consumed. In this regard its decomposition pathways and the fate of $Ru^{II}(bpy)_3^{2+}$ should be elucidated to design more efficient photocatalytic water oxidation systems. We found that two pathways exist for decomposition of $Ru^{II}(bpy)_3^{2+}$ in the light-$Ru^{II}(bpy)_3^{2+}$-$S_2O_8^{2-}$ system. The first is the formation of OH· radicals at pH > 6 through oxidation of OH^- by $Ru^{III}(bpy)_3^{3+}$ in the dark, which attack the bpy ligand of $Ru^{II}(bpy)_3^{2+}$. This is a minor, dark decomposition pathway. During irradiation not only $Ru^{II}(bpy)_3^{2+}$ but also $Ru^{III}(bpy)_3^{3+}$ also becomes photoexcited and the photoexcited $Ru^{III}(bpy)_3^{3+}$ reacts with $S_2O_8^{2-}$ to produce an intermediate which decomposes into catalytically active Ru μ-oxo dimers when the intermediate concentration is low or into catalytically inactive oligomeric Ru μ-oxo species

when the intermediate concentration is high. This is the major, light-induced decomposition pathway. When the $Ru^{II}(bpy)_3^{2+}$ concentration is low the light-$Ru^{II}(bpy)_3^{2+}$-$S_2O_8^{2-}$ system produces O_2 even in the absence of any added catalysts through the O_2 producing dark pathway. When the $Ru^{II}(bpy)_3^{2+}$ concentration is high, the system does not produce O_2 because the overall rate for the light-induced decomposition pathway is much faster than that of the O_2 producing dark pathway.

KEYWORDS: photocatalytic water oxidation, $Ru^{II}(bpy)_3^{2+}$, persulfate, decomposition pathways, fate

INTRODUCTION

In conjunction with the urgent need to develop alternative energy sources and materials, methods for homogeneous photocatalytic oxidation of water to form O_2 is receiving great attention. The most widely accepted system for this process consists of a water oxidation catalyst (Cat), photopump (PP) and sacrificial electron acceptor (sEA) (Scheme 1). Although a large number of catalysts and acceptors have been designed and tested for use in this system, only ruthenium trisbipyridine dication[1], $Ru^{II}(bpy)_3^{2+}$, and its derivatives[2,3] as the PP and persulfate, $S_2O_8^{2-}$, as the sEA have long been found to be effective to promote the water oxidation reaction.[2-13] The generally accepted mechanistic pathway for the photocatalytic water oxidation reaction promoted by this system is shown in Scheme 2a. In the route, absorption of light in the 400-500 nm region by $Ru^{II}(bpy)_3^{2+}$ brings about formation of a metal-to-ligand charge transfer (MLCT) excited state[14] (step 1, see the UV-vis spectrum of $Ru^{II}(bpy)_3^{2+}$ and the band assignments in Supporting Information Figure S1). In this transition, Ru(II) in $Ru^{II}(bpy)_3^{2+}$ is converted to Ru(III) along with movement of an electron

to the π* orbital of a bpy ligand. The formed MLCT excited state, denoted as $Ru^{III}(bpy)_2(bpy^{-\cdot})^{2+}$, is then oxidized by $S_2O_8^{2-}$ to produce $Ru^{III}(bpy)_3^{3+}$ (step 2) along with the sulfate anion radical ($SO_4^{-\cdot}$) and SO_4^{2-} (eq 1). The produced sulfate anion radical $SO_4^{-\cdot}$ then oxidizes another molecule of $Ru^{II}(bpy)_3^{2+}$ to generate $Ru^{III}(bpy)_3^{3+}$ (eq 2).

$$Ru^{III}(bpy)_2(bpy^{-\cdot})^{2+} + S_2O_8^{2-} \rightarrow Ru^{III}(bpy)_3^{3+} + SO_4^{-\cdot} + SO_4^{2-} \quad (1)$$

$$Ru^{II}(bpy)_3^{2+} + SO_4^{-\cdot} \rightarrow Ru^{III}(bpy)_3^{3+} + SO_4^{2-} \quad (2)$$

$$Ru^{III}(bpy)_2(bpy^{-\cdot})^{2+} + Ru^{II}(bpy)_3^{2+} + S_2O_8^{2-} \rightarrow 2\ Ru^{III}(bpy)_3^{3+} + 2\ SO_4^{2-} \quad (3)$$

In accord with previous findings,[15-18] photoinduced oxidation of two $Ru^{II}(bpy)_3^{2+}$ by $S_2O_8^{2-}$ yields two $Ru^{III}(bpy)_3^{3+}$ and two SO_4^{2-} (eq 3). Because oxidation of two water molecules to form O_2 and four protons (step 5) is a 4-electron process, four $Ru^{III}(bpy)_3^{3+}$ are required to carry out this reaction by oxidizing either four one-electron oxidation catalysts, two two-electron oxidation catalysts or four oxidizing centers in a four-electron oxidation catalyst (step 4) along with regeneration of four $Ru^{II}(bpy)_3^{2+}$.

Ideally, the above catalytic cycle would continue until all $S_2O_8^{2-}$ is consumed. However, despite the presence of excess amounts of $S_2O_8^{2-}$, the cycle usually proceeds for 10-15 min in a steady state[4-6] and stops much earlier before the sacrificial electron acceptor is fully consumed owing to fast decomposition of light absorbing $Ru^{II}(bpy)_3^{2+}$.[2-13] Despite being the subject of several past studies,[19] much still remains unknown about the decomposition pathway for and the fate of $Ru^{II}(bpy)_3^{2+}$ in Cat-$Ru^{II}(bpy)_3^{2+}$-$S_2O_8^{2-}$ promoted water oxidation reaction. As a result, decomposition of $Ru^{II}(bpy)_3^{2+}$ remains an important issue that needs to

be resolved in order to develop ideal photopumps and efficient water oxidation catalysts with high turnover numbers (TONs) and rates (TORs). Moreover, knowledge about this process should contribute significantly to the design of photocatalytic systems, which do not require sacrificial electron acceptors or donors.

In addition to issues regarding the fate of $Ru^{II}(bpy)_3^{2+}$ and its decomposition pathway, a fundamental question exists concerning whether or not $Ru^{III}(bpy)_3^{3+}$ can oxidize water without the assistance of Cats. This question arises because of the thought that if this complex oxidizes Cats it should have a sufficiently high potential to oxidize water directly. In the study described below, we have gained new insights into the decomposition pathways and fate of $Ru^{II}(bpy)_3^{2+}$ in the catalytic cycle for water oxidation. Significantly, we found that the key intermediate $Ru^{III}(bpy)_3^{3+}$ can oxidize water to produce O_2 in the absence of a Cat via one-electron oxidation of hydroxide.

RESULTS AND DISCUCSSION

The results of investigations using several experimental approaches have provided important information about the questions posed above. In the first experiments, production of O_2 as a function of $Ru^{II}(bpy)_3^{2+}$ concentrations ($[Ru^{II}(bpy)_3^{2+}]$) and time was evaluated. For this purpose, bicarbonate buffer solutions (pH = 9.6), containing a fixed (6 mM) concentration of $Na_2S_2O_8$ ($[S_2O_8^{2-}]$) and varying (0.005-0.6 mM) $[Ru^{II}(bpy)_3^{2+}]$ in a reactor (40 mL) containing a quartz window were irradiated for different time periods using a 1 Sun solar simulated light. Helium was used to continuously flush the solution during irradiation and so that the O_2 content of the output gas could be analyzed by using gas chromatography. The results of these experiments are summarized in the plots given in Figure 1. Specifically, the

rates (mol/h) of O_2 produced by water oxidation and total amount of O_2 produced with respect to time for reactions involving different [$Ru^{II}(bpy)_3^{2+}$] are summarized in the plots given in Figures 1a-c. As can be seen by viewing these plots, no O_2 gas is generated when [$Ru^{II}(bpy)_3^{2+}$] > 0.5 mM and O_2 begins to form as [$Ru^{II}(bpy)_3^{2+}$] decreases and reaches a maximum (5.3 μmol, Figure 1c) when [$Ru^{II}(bpy)_3^{2+}$] = 0.03 mM. At [$Ru^{II}(bpy)_3^{2+}$] below 0.03 mM the production of O_2 decreases rapidly. Under the conditions employed, the maximum rates of O_2 production occur around 0.75 h (Figure 1a). Furthermore, the existence of an initial O_2-generation free time period (0.25 h) is not a consequence of a required preliminary reaction (induction period) but rather it is associated with the need for O_2 formed in the medium to escape and fill the headspace of the reactor and be detected by GC. This conclusion is supported by the observation that the length of the initial O_2-free time period decreases as the size of the reactor decreases. Furthermore, by using an O_2 electrode immersed in the solution, we observe that O_2 production occurs immediately after the onset of irradiation (Figure 1d). Interestingly, as [$Ru^{II}(bpy)_3^{2+}$] increases, O_2 formed in the water oxidation reaction is initially consumed (Figure 1d). This observation suggests that the initially formed unstable intermediate Ru species undergo O_2-consuming polymerization when their concentrations are high.

A plot of the turnover number of O_2 and turnover number of oxidation versus [$Ru^{II}(bpy)_3^{2+}$] is shown in Figure 1e. Analysis of a plot of photochemical O_2 production at fixed [$Ru^{II}(bpy)_3^{2+}$] (0.03 mM) and [$Na_2S_2O_8$] (6 mM) as a function of pH in the range of 5-11 (Figure 1f) shows that the O_2 producing water oxidation reaction takes place only when the pH is higher than 5 and that the O_2 formation nearly linearly increases with increasing pH.

The results summarized above unequivocally demonstrate for the first time that photochemical O_2 production by oxidation of water using the $Ru^{II}(bpy)_3^{2+}$-$S_2O_8^{2-}$ couple

takes place at low [$Ru^{II}(bpy)_3^{2+}$] in the absence of added Cats. To further explore this process, three sets of solutions, buffered at pH = 6, 8 and 10 and containing $Ru^{III}(bpy)_3^{3+}$ (5 mM), were prepared and divided into two groups. To each sample in the first group was added amplex red (5 mM, Figure 2) and to each in the other set were added both amplex red (5 mM) and horseradish peroxidase (HRP). Amplex red is a reliable titrant for OH· because the reaction is associated with a rapid color change from colorless (amplex red) to deep purple (resorufin).[20] HRP specifically catalyzes the homolysis reaction of hydrogen peroxide (H_2O_2) to form two OH· radicals. As a result, the extent of formation of resorufin from amplex red in reactions occurring in the first group will indicate the amount of OH· radical generated while production of this substance in the second group of reactions will indicate the amounts of both H_2O_2 and free OH· radicals generated. The results arising from these experiments, summarized in Table 1, show that the dark reaction at pH = 6 leads to complete conversion of $Ru^{III}(bpy)_3^{3+}$ to $Ru^{II}(bpy)_3^{2+}$. As the pH of the reaction medium increases from 6 to 8 and then 10, the respective amounts of $Ru^{II}(bpy)_3^{2+}$ formed decrease to 95% and 82%. These observations show that decomposition of non $Ru^{II}(bpy)_3^{2+}$-producing $Ru^{III}(bpy)_3^{3+}$ occurs in the dark more efficiently at high pH. In addition, the results of colorimetric measurements demonstrate that at pH = 6, H_2O_2 and OH· radical are produced in respective yields of 10.5 and 4%, based on the initial amount of $Ru^{III}(bpy)_3^{3+}$ used. In contrast, at pH = 8, O_2 is generated as the major product (10%) and OH· radical and H_2O_2 are formed in respective 3.5 and 7.5 yields. Finally, at pH = 10, O_2 is the major product (25%) while H_2O_2 only a minor product (4.5%).

The results of these experiments show that H_2O_2 is the major product of $Ru^{III}(bpy)_3^{3+}$ promoted water oxidation at low pH and O_2 is the major product at high pH. The following

conclusions can be extracted from these observations. To accommodate the above results we prepared a new scheme (Scheme 2b) which contains four new steps (steps 6-9) in addition to the conventional scheme (Scheme 2a). Firstly, $Ru^{III}(bpy)_3^{3+}$ oxidizes water in the absence of a catalyst to produce O_2 via a single electron pathway that takes place through reaction between $Ru^{III}(bpy)_3^{3+}$ and OH^- to give the HO· radical (eq 4, step 6 in Scheme 2b), which then mainly dimerizes to produce H_2O_2 (eq 5, step 7 in Scheme 2b). However, at pH > 6, the OH· radials competitively react with $Ru^{II}(bpy)_3^{2+}$ to give a decomposition product (step 8 in Scheme 2b). We define this pathway (steps 6 and 8 in Scheme 2b) as the minor (or dark) decomposition pathway for $Ru^{III}(bpy)_3^{3+}$. Consistent with this proposal, are the earlier findings by Dutta[21, 22] that OH· radicals react with $Ru^{II}(bpy)_3^{2+}$ and by Creutz and Sutin[21, 22] that spontaneous reduction of $Ru^{III}(bpy)_3^{3+}$ takes place in aqueous solution to form $Ru^{II}(bpy)_3^{2+}$. Moreover, it is known that two $Ru^{III}(bpy)_3^{3+}$ ions react with H_2O_2 to give one O_2 molecule and two protons (eq 6, step 9 in Scheme 2b).[21,24] Indeed when the standard reaction with $[Ru^{II}(bpy)_3^{2+}]$ = 0.03 mM and $[Na_2S_2O_8]$ = 6 mM was carried out at pH = 10, the yield of O_2 dramatically increased in the presence of added hydrogen peroxide (Figure 3). Lastly, the newly added steps 6-9 in Scheme 2b take place only under the special conditions where $[Ru^{II}(bpy)_3^{2+}]$ is low and the pH is greater than 5.

$$Ru^{III}(bpy)_3^{3+} + OH^- \rightarrow Ru^{II}(bpy)_3^{2+} + OH\cdot \quad (4)$$

$$2\ OH\cdot \rightarrow H_2O_2 \quad (5)$$

$$2\ Ru^{III}(bpy)_3^{3+} + H_2O_2 \rightarrow 2\ Ru^{II}(bpy)_3^{2+} + O_2 + 2\ H^+ \quad (6)$$

$$OH\cdot + Ru^{II}(bpy)_3^{2+} \rightarrow \text{decomposed Ru complexes} \quad (7)$$

The next question addressed in this effort is why the yield of O_2 decreases with

increasing [$Ru^{II}(bpy)_3^{2+}$] in the photoinduced water oxidation reaction (Figure 1c). To gain information about this issue, UV-vis spectroscopy was employed to monitor changes taking place in the reaction performed using [$Ru^{II}(bpy)_3^{2+}$] = 0.03 and [$S_2O_8^{2-}$] = 0.6 mM (Figure 4) at pH = 10. The results show that the intensity of the MLCT absorption band of $Ru^{II}(bpy)_3^{2+}$ (Figure 4a) decreases rapidly (>75%) within 0.5 min (Figure 4b) upon irradiation of the solution with a solar simulated light and completely disappears after 2.5 min (Figure 4c). After this period, two new absorption bands appear at ca. 450 and ca. 580 nm, which finally become well-resolved maxima at 480 and 630 nm (Figure 4d). In comparison with the authentic spectra (Figure 4e) they are assigned as the orange dimer $(bpy)_2(H_2O)Ru^{III}$-O-$Ru^{IV}(H_2O)(bpy)_2$ (450 nm band, denoted as Ru_2(III,IV)) and the blue dimer $(bpy)_2(H_2O)Ru^{III}$-O-$Ru^{III}(H_2O)(bpy)_2$ (580 nm band, denoted as Ru_2(III,III)).[25-29] Thus, during the photoreaction $Ru^{II}(bpy)_3^{2+}$ is rapidly transformed to orange and blue dimers. We isolated the single crystals of Ru_2(III,IV) and determined its structure in two different lattice systems, monoclinic and triclinic (Table 2). In this structure two H_2O molecules coordinated to two Ru atoms in Ru_2(III,IV) were replaced by two sulfate ions (SO_4^{2-}) giving rise to a related structure, $\{[Ru^{III}(SO_4)(bpy)_2](\mu\text{-}O)[Ru^{IV}(SO_4)(bpy)_2]\}^+$. In the monoclinic structure the oxidation states of Ru atoms are equivalent (+3.5) and the two $Ru^{III/IV}$-(μ-O) distances are equal (1.838(9) Å). In the triclinic structure (Figure 5a, see Table S1, Figure S2 and Figure S3 in the Supporting Information for further details) the two Ru atoms have +3 and +4 oxidation states, and accordingly the Ru-(μ-O) distances are nonequivalent (Ru^{III}-(μ-O) = 1.856(6) and Ru^{IV}-(μ-O) = 1.820(6) Å). Although the structure of Ru_2(III,III) is already known by Meyer and his coworkers[28] we also obtained its single crystals and newly determined its crystal structure using a synchrotron radiation source (Table 2, Table S2, and Figure S4 in the

Supporting Information). The two Ru^{III}-(μ-O) distances of the newly obtained Ru_2(III,III) are equal (1.869(8) Å) and the distance coincides with the literature report.[28]

It is well known that Ru_2(III,III) is oxidized to Ru_2(V,V), the ultimate water oxidation catalyst, by strong one-electron oxidants such as $Ru^{III}(bpy)_3^{3+}$. Many intermediates exist in the pathway for this oxidation process, including Ru_2(III,IV), which along with Ru_2(III,III) are the precursors of Ru_2(V,V). Accordingly, both dimers promote water oxidation through the processes described in steps 14 and 15 in Scheme 2b. We confirmed that both dimers catalyze the water oxidation reaction using $[Ru^{II}(bpy)_3^{2+}]$ = 0.03 and $[S_2O_8^{2-}]$ = 0.6 mM and showed that much larger amounts of O_2 are generated than when these dimers are not present (Figure 6a). Likewise, if the Ru species that remain in the solution following complete decomposition of $Ru^{II}(bpy)_3^{2+}$ are indeed the blue and orange dimers, then O_2 forming water oxidation should resume when $Ru^{II}(bpy)_3^{2+}$ is added. Indeed, addition of an aliquot of $Ru(bpy)_3^{2+}$, which corresponds to 0.03 mM, to the solution generated following the first cycle leads to formation of larger amounts of O_2 (Figure 6b). The O_2 production enhancement effect caused by addition of $Ru(bpy)_3^{2+}$ continues until the fourth cycle but sharply decreases thereafter. During each reaction cycle, the 630 nm band associated with the blue dimer progressively red shifts to 670 nm and its intensity increases (Figure 6c). Simultaneously, the 480 nm band associated with the orange dimer progressively blue shifts to ca. 450 nm. We conclude that the strong peak at 610 nm (Figure 6c, black spectrum) arises from a catalytically inactive oligomeric Ru species Ru_n ($n \geq 3$). This proposal gains support from the observation that the trinuclear Ru complex, $\{[Ru^{III}(SO_4)(bpy)_2(\mu\text{-}O)]_2Ru^{IV}(bpy)(H_2O)_2\}$, is isolated from the reaction mixture after the fourth cycle and characterized by using x-ray crystallography (Figure 5b, Table 2, S5 and S6 in the Supporting Information). In the structure each SO_4^{2-} ion coordinates to the terminal Ru(III) through an O

atom and to two H_2O molecules coordinated to the middle Ru^{IV} through two H-bonding.

In conjunction with the above findings, we observed that when [$Ru^{II}(bpy)_3^{2+}$] is increased from 0.03 to 0.3 mM while keeping [$S_2O_8^{2-}$] at 0.6 mM, no O_2 is generated even in the first cycle (Figure 6b, red trace). Moreover, the Ru species formed in the first cycle under these conditions do not promote water oxidation during the second cycle. These phenomena are a consequence of the fact that when [$Ru^{II}(bpy)_3^{2+}$] is high, the initially formed unstable intermediate Ru species derived from $Ru^{II}(bpy)_3^{2+}$ very rapidly form catalytically inactive oligomeric and/or polymeric Ru species, Ru_n ($n \geq 3$).

Even when the initial [$Ru^{II}(bpy)_3^{2+}$] is high, such as 0.3 mM, the concentration of $Ru^{II}(bpy)_3^{2+}$ at the elapsed time of t [$Ru^{II}(bpy)_3^{2+}$]$_t$ will eventually drop down to ~0.03 mM after undergoing a series of decomposition and polymerization processes. When [$Ru^{II}(bpy)_3^{2+}$] reaches such active concentrations then O_2 is expected to be generated. In the reality, however, O_2 is never produced. This indicates that the catalytically inactive oligomeric and polymeric Ru species, Ru_n ($n \geq 3$), once formed, very rapidly consumes the newly formed unstable intermediate Ru species for them to grow bigger or very rapidly catalyze oligomerization and polymerization of the newly formed unstable intermediate Ru species into Ru_n ($n \geq 3$).

In additional studies, we found that $Ru^{II}(bpy)_3^{2+}$ and $Ru^{III}(bpy)_3^{3+}$ undergo decomposition only when $S_2O_8^{2-}$ is present in the irradiated mixture but not when only H_2O_2 is present, nor in the dark even in the presence of $S_2O_8^{2-}$, and finally regardless of the pH. In addition, $Ru^{III}(bpy)_3^{3+}$ is extremely stable in the dark at pH = 3, even in the presence of either $S_2O_8^{2-}$ or H_2O_2. Even at pH = 6, all of $Ru^{III}(bpy)_3^{3+}$ is converted to $Ru^{II}(bpy)_3^{2+}$ (Figure 7, Table 1). However, upon irradiation in the presence of $S_2O_8^{2-}$, it rapidly undergoes reaction to form the orange dimer (Figure 8a-d). The UV-vis spectrum of the authentic orange dimer

(Figure 8e) supports the above phenomenon. Thus, both light and $S_2O_8^{2-}$ are essential not only for the formation of $Ru^{III}(bpy)_3^{3+}$ but also for its rapid decomposition.

Based on the combined results, we conclude that the process involving ultimate production of catalytically inactive oligomeric and/or polymeric Ru species is the major (or light-induced) decomposition pathway for $Ru^{II}(bpy)_3^{2+}$ during the water oxidation reaction in the presence of $S_2O_8^{2-}$. The proposed comprehensive route shown in Scheme 2b plausibly accounts for the fate of $Ru^{II}(bpy)_3^{2+}$ during the reaction. In this pathway, $Ru^{III}(bpy)_3^{3+}$ undergoes photoinduced ligand-to-metal charge transfer (LMCT) to form $Ru^{II}(bpy)_2(bpy^{+\bullet})^{3+}$ (step 10), which then undergoes MLCT from Ru(II) to a bpy ligand (step 11) to give rise to $[Ru^{III}(bpy)(bpy^{-\bullet})(bpy^{+\bullet})]^{3+}$. This Ru intermediate is readily oxidized by $S_2O_8^{2-}$ to give $Ru^{III}(bpy)_2(bpy^{+\bullet})^{4+}$ (step 12), which then dimerizes to form Ru(III,III) and Ru(III,IV) when its concentration is low (step 13). In contrast, oligomeric Ru_n ($n \geq 3$) is generated from Ru(III,III) and Ru(III,IV) (step 16) when $[Ru^{II}(bpy)_3^{2+}]$ is high (> 0.1 mM). Furthermore, because the rates for oligomerization and/or polymerization (step 16) are much larger than that for dimerization (step 13), and the combined rates for steps 10-12 and 16 are much larger than that for oxidation of OH^- by $Ru^{III}(bpy)_3^{3+}$ (step 6), fast decomposition of $Ru^{II}(bpy)_3^{2+}$ occurs in the irradiation-induced reaction in the presence of $S_2O_8^{2-}$.

CONCLUSIONS

In summary, we report that two pathways exist for decomposition of $Ru^{II}(bpy)_3^{2+}$ in the light-$Ru^{II}(bpy)_3^{2+}$-$S_2O_8^{2-}$ system. The first is the formation of OH· radicals at pH > 6 through oxidation of OH^- by $Ru^{III}(bpy)_3^{3+}$ in the dark, which attack the bpy ligand of $Ru^{II}(bpy)_3^{2+}$. This is a minor, dark decomposition pathway. When the system is under the irradiation

condition not only $Ru^{II}(bpy)_3^{2+}$ but also generated $Ru^{III}(bpy)_3^{3+}$ also becomes photoexcited and subsequently the photoexcited $Ru^{III}(bpy)_3^{3+}$ reacts with $S_2O_8^{2-}$ to produce an intermediate which decomposes into catalytically active Ru μ-oxo blue and orange dimers when the intermediate concentration is low or into catalytically inactive oligomeric Ru μ-oxo species when the intermediate concentration is high. This is the major, light-induced decomposition pathway. The proposed intermediate in the route for light-induced decomposition of $Ru^{II}(bpy)_3^{2+}$ is $Ru^{III}(bpy)_2(bpy^{+\bullet})^{4+}$.

The dark decomposition pathway is a consequence of the ability of $Ru^{III}(bpy)_3^{3+}$ to oxidize hydroxide ion (OH^-) via a single electron oxidation mechanism to yield OH· radicals, which subsequently dimerize to form H_2O_2. $Ru^{III}(bpy)_3^{3+}$ then oxidizes H_2O_2 to yield an O_2 molecule and two protons. We define this pathways as the catalyst-free O_2 producing dark pathway that operates only when the concentration of $Ru^{II}(bpy)_3^{2+}$ is low (< 0.2) at pH > 6. Therefore, when the $Ru^{II}(bpy)_3^{2+}$ concentration is low the light-$Ru^{II}(bpy)_3^{2+}$-$S_2O_8^{2-}$ system produces O_2 even in the absence of any added catalysts through the O_2 producing dark pathway. However, when the $Ru^{II}(bpy)_3^{2+}$ concentration is high, the system does not produce O_2 via the catalyst-free O_2 producing dark pathway because the overall rate for the light-induced decomposition pathway is much faster than that of the catalyst-free O_2 producing dark pathway.

We believe that the observations made in this study and the conclusion drawn provide a greater understanding of the role played by $Ru^{II}(bpy)_3^{2+}$ as a photopump or photosensitizer for photocatalytic water oxidation reactions. Our findings should serve as useful guidelines for future designs of stable photosensitizing or photopumping systems including molecular artificial photosynthetic systems.

EXPERIMENTAL METHODS

Materials. Tris(2,2′–bipyridyl)ruthenium (II) chloride hexahydrate, (~98%) was purchased from Strem Chemicals and sodium peroxodisulfate was purchased from Junsei Chemical Co. Ltd. Ampliflu Red™, horseradish peroxidase and resorufin were purchased from Sigma-Aldrich. The materials for the preparation of buffer solutions, Na_2SiF_6, $NaHCO_3$, and Na_2CO_3 were purchased from Aldrich. The buffer solutions with pH = 5~8 were prepared by mixing Na_2SiF_6 and $NaHCO_3$ to a desired pH and those with pH = 9~11 were prepared by mixing $NaHCO_3$ and Na_2CO_3 to a desired pH. The total concentration of the mixed salts was fixed to 0.1 M.

Water oxidation reaction. Bicarbonate buffer solutions (pH = 9.6), containing a fixed (6 mM) concentration of $Na_2S_2O_8$ ($[S_2O_8^{2-}]$) and varying (0.005-0.6 mM) $[Ru^{II}(bpy)_3^{2+}]$ in a reactor (40 mL) containing a quartz window were irradiated for different time periods using a 1 Sun solar simulated light. The solution was magnetically stirred continuously and degassed with He (99.9999 %) for 2 h in the dark to remove residual O_2 before the irradiation starts. Helium was used to continuously flush the solution during irradiation and so that the O_2 content of the output gas could be analyzed by using gas chromatography. A standard AM-1.5 solar simulated light (HAL-302 Asahi) with the power of 100 mW cm^{-2} was used as the light source. The light intensity was monitored using a 1-sun checker (CS-20, Asahi Spectra Co., Ltd.).

O_2 measurement. The gas chromatographic analysis of O_2 was conducted on a Young-Lin YL6500 GC equipped with a pulsed discharge detector (PDD). A molecular sieve column (30 m × 0.53 mm, 25 mm pore) was used and the oven temperature was isothermally kept at 40 °C. The flow rate of the carrier gas (helium) was maintained at 6 mL min^{-1}. A standard O_2

gas (0.1% in Ar) was used as the standard to quantitatively analyze the concentration of O_2 in the gas stream. Pro ODO (digital Professional Series YSI) was used for the measurements of the concentrations of dissolved oxygen. A diode array UV-vis spectroscopy S-3100 (Sinco) and Cary 5000UV-Vis-NIR spectrophotometer (Varian) were used for the spectroscopic measurements. For the kinetics of oxygen evolution (Figure 1d) an Ocean Optics oxygen sensor (FOXY-OR125-G) interfaced to a PC was used. The probe was calibrated prior to use before introducing $Ru(bpy)_3^{2+}$ or $Ru(bpy)_3^{3+}$ into the chamber containing the standard buffer solution. We confirmed no O_2 evolution in the absence of any $Ru(bpy)_3^{3+}$ or $Ru(bpy)_3^{2+}$.

Measurement of H_2O_2 and OH· radical. Amplex red and horseradish peroxidase (HRP) were used for the measurements of H_2O_2 and $OH^{\cdot}$ radical. The stock solution of amplex red was prepared in dimethyl sulfoxide (DMSO) and stored at -20^0C until use. 1 mg of amplex red was dissolved in 2.5 mL DMSO and 0.2 mL was taken for the detection of H_2O_2 and OH· for each titration of the OH· in the solution. The stock solution of HRP was made by dissolving 1 mg of HRP in 2.5 mL of 1 M phosphate buffer. For the detection of H_2O_2 0.1 mL of the HRP solution was taken.

Preparation of Ru_2(III,III), Ru_2(III,IV), and a Ru_3(III,IV,III) complex. The blue crystals of Ru_2(III,III) were obtained according to the literature report.[30] The dark orange crystals of Ru_2(III,IV) were obtained by dissolving Ru_2(III,III) and $Na_2S_2O_8$ in water with the molar ratio of 1:4 at room temperature followed by slow evaporation of water at room temperature (Figure 5a). For the isolation of the green crystals of Ru_3(III,IV,III) the water oxidation reaction was repeated for five times in a large scale (1 L) under the standard condition ($[S_2O_8^{2-}]$ = 6 mM) and $[Ru^{II}(bpy)_3^{2+}]$ = 0.03 mM). The dark green solution (5 L) was concentrated under the reduced pressure using rotary evaporator (bath temp. 20 ~ 25 ℃).

The residual solid was dispersed in ethanol and white precipitate ($NaCO_3$, $NaHCO_3$) was removed by filtration using a membrane filter (0.2 ㎛, Millipore Co.). The filtrate was concentrated under reduced pressure. The concentrated reddish green residue was dispersed in small amount of ethanol and filtered again using a membrane filter. The remaining green solid was dispersed in ethanol, which became a sticky solid. This was dissolved with a minimum amount of ethanol and then kept it at room temperature for slow evaporation. When most of ethanol was evaporated green crystals appeared. Among them we found a Ru trimer complex shown in Figure 5b.

Crystal structure determination. Each single crystal of Ru_2(III,III) (0.020 × 0.020 × 0.010 mm^3), Ru_2(III,IV) (0.008 × 0.008 × 0.005 mm^3), and Ru_3(III,IV,III) complex (0.010 × 0.010 × 0.008 mm^3) was mounted on a holder with the help of an optical microscope. X-ray diffraction patterns were recorded on a ADSC Quantum 210 CCD diffractometer using synchrotron radiation (λ = 0.7000 Å), with a scan width of 1.00° in ω angle rotation, scanning times of 2, 30, and 10 sec, respectively, per frames using ADSC Q210 ADX program.[31] These measurements were conducted in Macromolecular Crystallography Wiggler Beamline 2D, Pohang Accelerator Laboratory (PAL). The structure refinements of all single crystals (blue, orange, and green) were modified the radiation wavelength 0.7000 Å using the instruction of DISP (the dispersion and the absorption coefficient of particular elements) in SHELXTL program.[32] The crystal data and structure refinements are summarized in Table S1. All independent atoms were refined anisotropically.

ASSOCIATED CONTENT

AUTHOR INFORMATION

Corresponding author
yoonkb@sogang.ac.kr

Notes
The authors declare no competing financial interest.

Present Addresses
†Institution of Glass and Ceramic Research Division, Bangladesh Council of Scientific and Industrial Research (BCSIR), Dr. Qudraat-i-khuda Road, Dhanmondi, Dhaka, Bangladesh.

Supporting Information
Details of the structural data of the Ru species and the analysis of the UV-vis spectrum of $Ru(bpy)_3^{2+}$ in an aqueous solution. This material is available free of charge via the Internet at http://pubs.acs.org

ACKNOWLEDGMENTS
This study was financially supported by the Korea Center for Artificial Photosynthesis, located at Sogang University and funded by the Ministry of Science, ICT and Future Planning through the National Research Foundation of Korea, No. 2009-0093886. We also thank Jiyun Lee for help for drawing Table of Content and Figures 1 and 2.

References
(1) Demas, J. N.; Adamson, A. W. *J. Am. Chem. Soc.* **1971**, *93*, 1800–1801.

(2) Duan, L.; Xu, Y.; Zhang, P.; Wang, M.; Sun, L. *Inorg. Chem.* **2010**, *49*, 209–215.
(3) Xu, Y.; Duan, L.; Tong, L.; Åkermarkb, B.; Sun, L. *Chem. Commun.,* **2010**, *46*, 6506–6508.
(4) Li, F.; Jiang, Y.; Zhang, B.; Huang, F.; Gao, Y.; Sun, L. *Angew. Chem. Int. Ed.* **2012**, *51*, 2417–2420.
(5) Duan, L. ; Bozoglian, F.; Mandal, S.; Stewart, B.; Privalov, T.; Llobet, A.; Sun, L. *Nat. Chem.* **2012**, *4*, 418–423.
(6) Lewandowska-Andralojc, A.; Polyansky, D. E.; Zong, R.,; Thummel, R. P.; Fujita, E. *Phys. Chem. Chem. Phys.* **2013**, *15*, 14058–14068.

(7) Kärkäs, M.; Verho, D. O.; Johnston, E. V.; Åkermark, B. *Chem. Rev.* **2014**, *114*, 11863−12001.

(8) Concepcion, J. J.; Jurss, J. W.; Kylebrennaman, M.; Hoertz, P. G.; Patrocinio, A. O. T.;

Iha, N. Y. M.; Templeton, J. L.; Meyer, T. J. *Acc. Chem. Res.* **2009**, *42*, 1954–1965.

(9) Kim, W.; McClure, B. A.; Edri, E.; Frei, H. *Chem. Soc. Rev.* **2016**, *45*, 3221–3243.

(10) Young, K. J.; Martini, L. A.; Milot, R. L.; Snoeberger III, R. C.; Batista, V. S.; Schmuttenmaer, C. A.; Crabtree, R. H.; Brudvig, G. W. *Coord. Chem. Rev.* **2012**, *256*, 2503–2520.

(11) Sartorel, A.; Bonchio, M.; Campagnab, S.; Scandola, F. *Chem. Soc. Rev.* **2013**, *42*, 2262–2280.

(12) Neudeck, S.; Maji, S.; López, I.; Meyer, S.; Meyer, F.; Llobet, A. *J. Am. Chem. Soc.* **2014**, *136*, 24−27.

(13) Liu, Y.; Ng, S.-M.; Yiu, S. M.; Lam, W. W. Y.; Wei, X. G.; Lau, K.-C.; Lau, T. C. *Angew. Chem. Int. Ed.* **2014**, *53*, 14468 –14471.

(14) Lytle, F. E.; Hercules, D. M. *J. Am. Chem. Soc.* **1969**, *91*, 253–257.

(15) Neumann-Spallart, M.; Kalyanasundaram, K.; Grätzel, C.; Grätzel, M. *Helv. Chim. Acta,* **1980**, *63*, 1111–1118.

(16) Bolletta, F.; Juris, A.; Maestri, M.; Sandrini, D. *Inorg. Chim.* Acta, **1980**, *44*, L175–L176.

(17) Harriman, A.; Porter, G.;Walters, P. *J. Chem. Soc. Faraday Trans.* 2, **1981**, *77*, 2373–2383.

(18) Humphry-Baker, R.; Lilie, J.; Grätzel, M. *J. Am. Chem. Soc.* **1982,** *104,* 422–425.

(19) Armandi, M.; Hernandez, M. S.; Vankova, S.; Zanarini, S.; Bonelli, B.; Garrone, E. *ACS Catal.* **2013**, *3*, 1272−1278.

(20) Mishina, V.; Gray, J. P.; Heck, D. E.; Laskin, D. L.; Laskind, J. D. *Free Radic. Biol. Med*. **2010**, *48*, 1485–1491.

(21) Ledney, M.; Dutta, P. K. *J. Am. Chem. Soc.* **1995**, *117*, 7687–7695.

(22) Vaidyalingam, A.; Dutta, P. K. *Anal. Chem*. **2000**, *72*, 5219–5224.

(23) Creutz, C.; Sutin, N. *Proc. Nat. Acad. Sci.* **1975**, *72*, 2858–2862.

(24) Ghosh, P. K.; Brunschwig, B. S.; Chou, M.; Creutz, C.; Sutin, N. *J. Am. Chem. Soc.* **1984**, *106,* 4772–4783.

(25) Gersten, S. W.; Samuels, G. J.; Meyer, T. J. *J. Am. Chem. Soc.* **1982**, *104,* 4029–4030.

(26) Ellis, C. D.; Gilbert, J. A.; Murphy, Jr. W. R.; Meyer, T. J. *J. Am. Chem. Soc.* **1983**, *105,* 4842–4843.

(27) Lay, P. A.; Sasse, W. H. F. *Inorg. Chem.* **1983**, *24,* 4707–4710.

(28) Rotzinger, F. P.; Munavalli, S.; Comte, P.; Hurst, J. K.; Cratzel, M.; Pern, F.-J.; Frank, A. J. *J. Am. Chem. Soc.* **1987**, *109*, 6619–6626.

(29) Comte, P.; Naseeruddin, M. K.; Rotzinger, F. P.; Frank, A. J.; Grätzel, M. *J. Mol. Catal.*, **1989**, *52*, 63–84.

(30) Gilbert, J. A.; Eggleston, D. S.; Murphy, Jr. W. R.; Geselowitz, D. A.; Gersten, S. W.; Hodgson, D. J.; Meyer, T. J. *J. Am. Chem. Soc.* **1985**, ***107***, 3855–3864.

(31) Arvai, A. J. & Nielsen, C. ADSC Quantum-210 ADX Program, Area Detector System Corporation, Poway, CA, USA, 1983.

(32) Sheldrick, G. M. SHELXTL-PLUS, Crystal Structure Analysis Package, Bruker Analytical X-Ray, Madison, WI, USA, 1997.

Table 1. Products obtained from $Ru(bpy)_3^{3+}$ from the aqueous solutions of different pH.

pH	Initial $[Ru^{III}]$, μM	Returned $[Ru^{II}]$, μM	Unreturned $[Ru^{II}]$, μM / (%)	Products μM			
				O_2*[1]	OH·*[1]	H_2O_2*[1]	Total equivalent by $[Ru^{III}]$, μM (Yield %)
6	5	5.0	0.0 (0)	0.0	0.2	0.53	1.26 (25.2)
8	5	4.8	0.2 (4)	0.5	0.2	0.38	2.64 (52.8)
10	5	4.1	0.9 (18)	1.1	0.0	0.22	4.84 (96.8)

*[1]Total equivalent by $[Ru^{III}]$ is 4 for O_2, 1 for OH·, and 2 for H_2O_2.

Table 2. Crystal structure data and structure refinement for Ru-complexes (Blue dimer, orange dimer, and green trimer).

	Blue Dimer*[1]	Orange Dimer		Green Trimer
Chemical formula	$\{[Ru^{III}(H_2O)(bpy)_2]_2(\mu\text{-}O)\}\cdot(ClO_4^-)_4\cdot(H_2O)_2$	$\{[Ru^{III/IV}(SO_4^{2-})(bpy)_2]_2(\mu\text{-}O)\}\cdot(ClO_4^-)_2\cdot(H_9O_4^+)\cdot(H_2O)_3$	$\{[Ru^{III}(SO_4^{2-})(bpy)_2](\mu\text{-}O)[Ru^{IV}(SO_4^{2-})(bpy)_2]\}\cdot(ClO_4^-)_2\cdot(H_9O_4^+)\cdot(H_2O)_3$	$\{[Ru^{III}(SO_4)(bpy)_2(\mu\text{-}O)]_2Ru^{IV}(bpy)(H_2O)_2\}(OH)(HSO_4)(H_2O)_4(CH_3CH_2OH)$
Formula sum	$C_{40}H_{60}Cl_4N_8O_{21}Ru_2$	$C_{40}H_{47}Cl_2N_8O_{24}Ru_2S_2$	$C_{40}H_{47}Cl_2N_8O_{24}Ru_2S_2$	$C_{52}H_{60}N_{10}O_{22}Ru_3S_3$
Formula weight	1312.74 g/mol	1361.01 g/mol	1361.01 g/mol	1576.49 g/mol
Crystal system	monoclinic	monoclinic	triclinic	orthorhombic
Space-group	$C2_1/c$ (No. 15)	$C2_1/c$ (No. 15)	P -1 (No. 2)	$P\,2_12_12_1$ (No. 19)
Cell parameters	a = 22.701(5) Å b = 13.112(3) Å, c = 20.046(4) Å, β = 122.72(3)°	a = 12.621(3) Å b = 20.342(4) Å, c = 19.406(4) Å, β = 94.04(3)°	a=11.917(2) Å, b=12.022(2) Å, c=19.406(4) Å, α=91.80(3)° β=92.45(3)° γ=116.37(3)°	a=10.4320(21) Å b=20.8010(42) Å c=28.6870(57) Å
Z, Cell volume	4, 5020(2) Å^3	4, 4969.8(17) Å^3	2, 2484.7(10) Å^3	4, 6225(2) Å^3
Calc. density	1.737 g/cm^3	1.819 g/cm^3	1.819 g/cm^3	1.682 g/cm^3
Index ranges	$-27 \le h \le 27$, $-16 \le k \le 16$, $-24 \le l \le 24$	$-17 \le h \le 17$, $-28 \le k \le 28$, $-27 \le l \le 26$	$-14 \le h \le 14$, $-14 \le k \le 14$, $-23 \le l \le 23$	$-14 \le h \le 14$, $-29 \le k \le 29$, $-40 \le l \le 40$
Reflections collected	16826	24367	16685	59894
Independent reflections	4880 [R(int) = 0.0285]	6904 [R(int) = 0.1208]	8473 [R(int) = 0.0334]	181316 [R(int) = 0.1156]
Completeness	98.8 % (θ = 25.59°)	95.1 % (θ = 29.50°)	92.5 % (θ = 24.99°)	98.8 % (θ = 25.59°)
Max. and min. transmission	0.9986 and 0.9813	0.996 and 0.992	0.996 and 0.992	0.993 and 0.992
Data / restraints / parameters	4880 / 0 / 340	2887 / 0 / 355	8473 / 0 / 704	18298 / 781 / 745
Goodness-of-fit on F^2	1.052	1.050	1.059	0.956
Final R indices [I>2sigma(I)]	R_1 = 0.0349, wR_2 = 0.0950	R_1 = 0.1010, wR_2 = 0.2609	R_1 = 0.0863, wR_2 = 0.2403	R_1 = 0.0824, wR_2 = 0.2010
R indices (all data)	R_1 = 0.0366, wR_2 = 0.0966	R_1 = 0. 1367, wR_2 = 0.2912	R_1 = 0.1058, wR_2 = 0.2544	R_1 = 0.1897, wR_2 = 0.2611
CCDC No.*[2]	1476028	1476030	1476029	1476031

[1]Newly obtained in this work.[2]The crystal data can be obtained free of charge from the Cambridge Crystallographic Data Centre via www.ccdc.cam.ac.uk/data_request/cif.

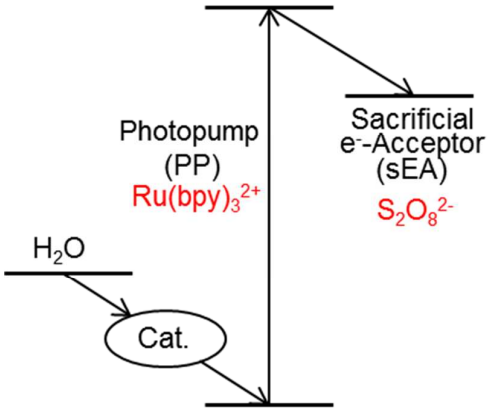

Scheme 1. The general scheme for water oxidation reaction in the presence of a catalyst (Cat), a photopump (PP), a sacrificial electron acceptor (sEA), and their roles.

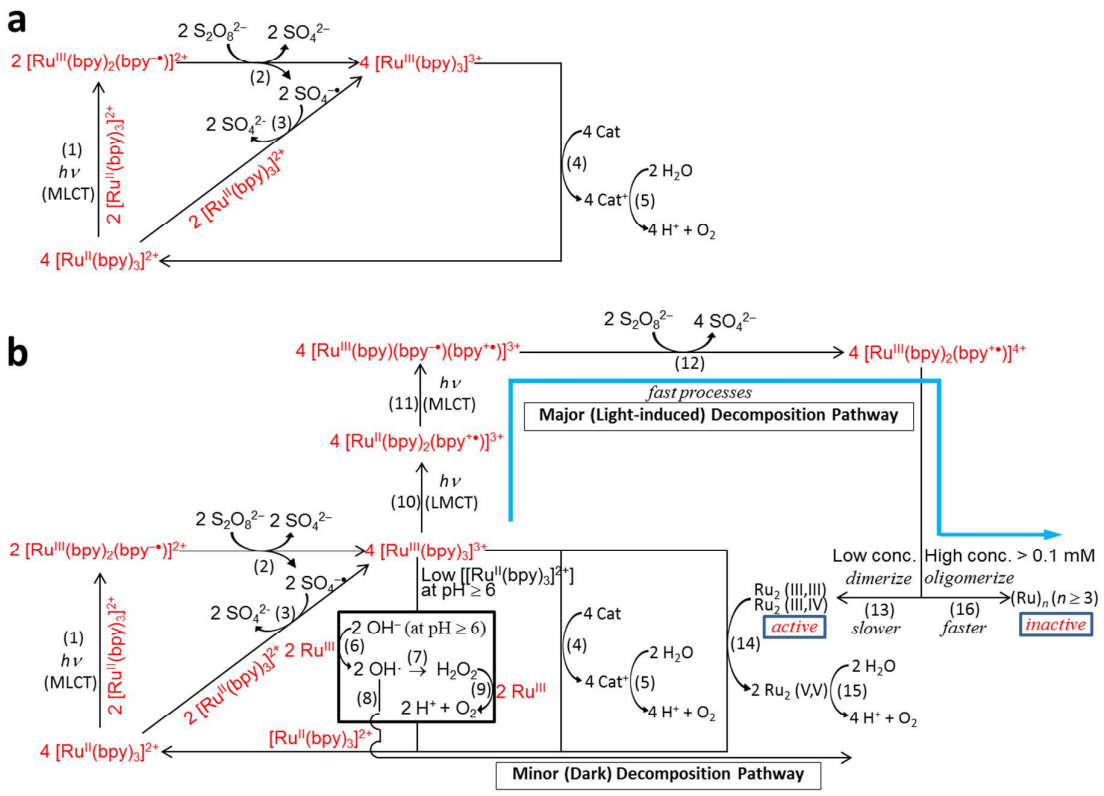

Scheme 2. The schemes for water oxidation reaction in the presence of a catalyst (Cat), $Ru(bpy)_3^{2+}$ as a photopump (PP), and persulfate, $S_2O_8^{2-}$, as a sacrificial electron acceptor (sEA). (a) Traditionally accepted simple scheme and (b) newly elucidated more comprehensive scheme.

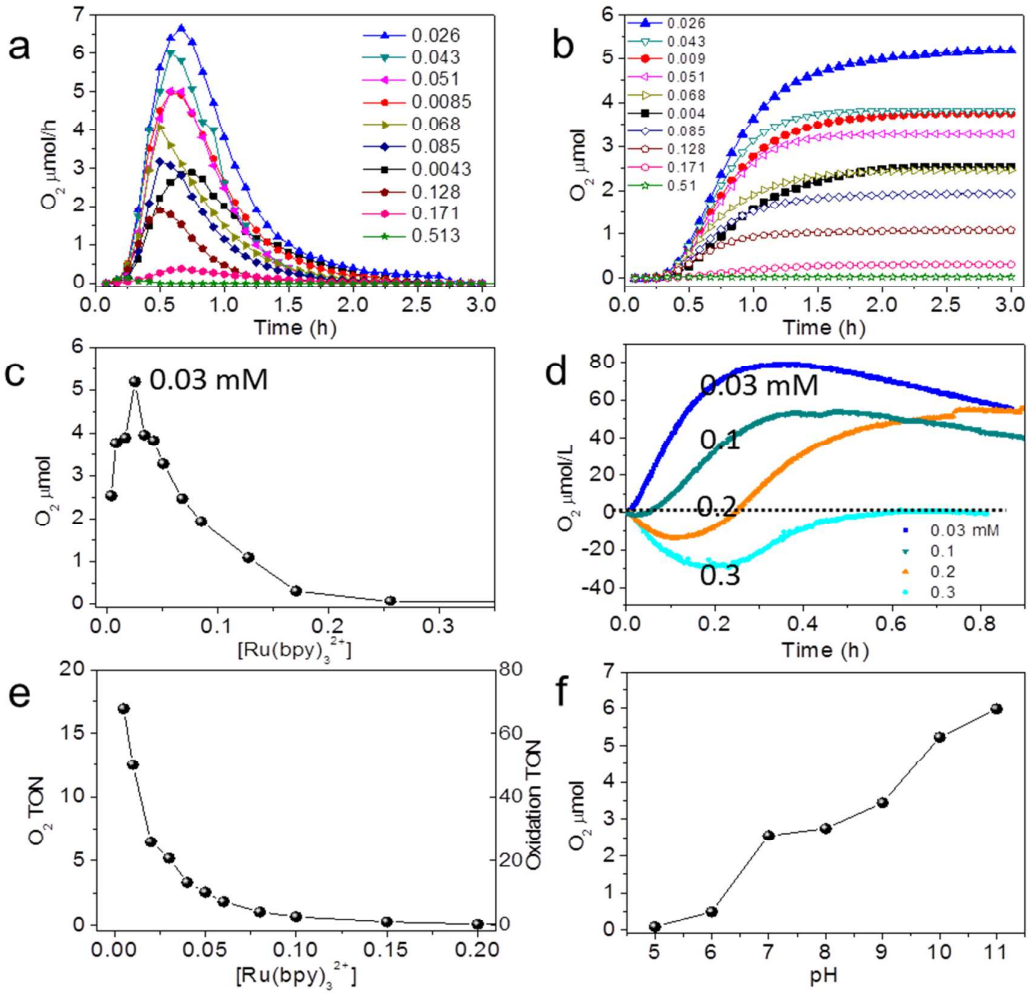

Figure 1. (a) The profile of visible light induced production of O_2 from $Ru(bpy)_3^{2+}$ (x mM) in the presence of $S_2O_8^{2-}$ (6 mM) with x between 0.004 and 0.51. (b) The plot of the cumulative amount of O_2 with respect to time. (c) The plot between the total amount of O_2 with respect to the concentration of $Ru(bpy)_3^{2+}$. (d) The profile of O_2 dissolved in the reaction mixture consisting of $Ru(bpy)_3^{2+}$ (x mM) and $S_2O_8^{2-}$ (6 mM) for x = 0.03, 0.1, 0.2, and 0.3, respectively. The dissolved amount of O_2 was detected using an O_2 electrode. (e) The plots of O_2 turnover number (O_2 TON) and oxidation turnover number (Oxdation TON) with respect to the concentration of $Ru(bpy)_3^{2+}$ (mM). (f) The plot of the produced amount of O_2 with respect to pH of the solution during the visible light induced production of O_2 from $Ru(bpy)_3^{2+}$ (0.3 mM) in the presence of $S_2O_8^{2-}$ (6 mM).

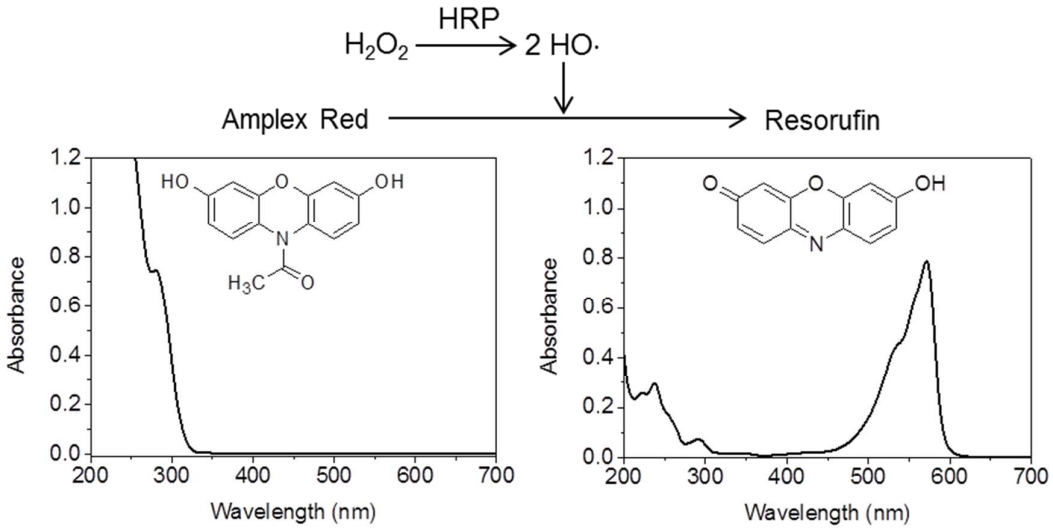

Figure 2. UV-Vis spectra of amplex red and resorufin and the scheme to detect OH· radical and H_2O_2.

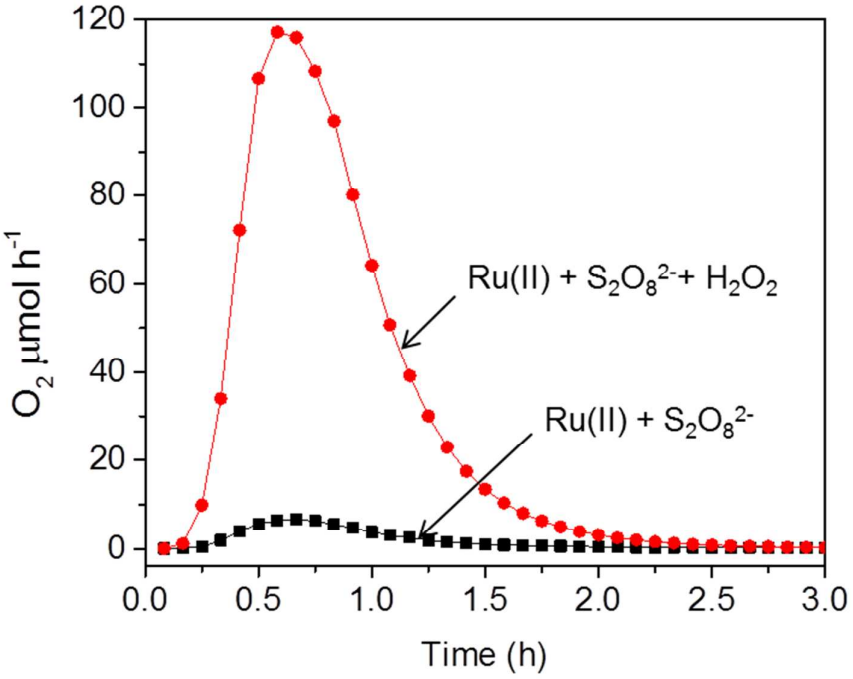

Figure 3. The reaction profiles of the visible light-induced O_2 production from the reaction mixtures consisting of $Ru(bpy)_3^{2+}$ and $S_2O_8^{2-}$ (black) and $Ru(bpy)_3^{2+}$, $S_2O_8^{2-}$, and H_2O_2 (red).

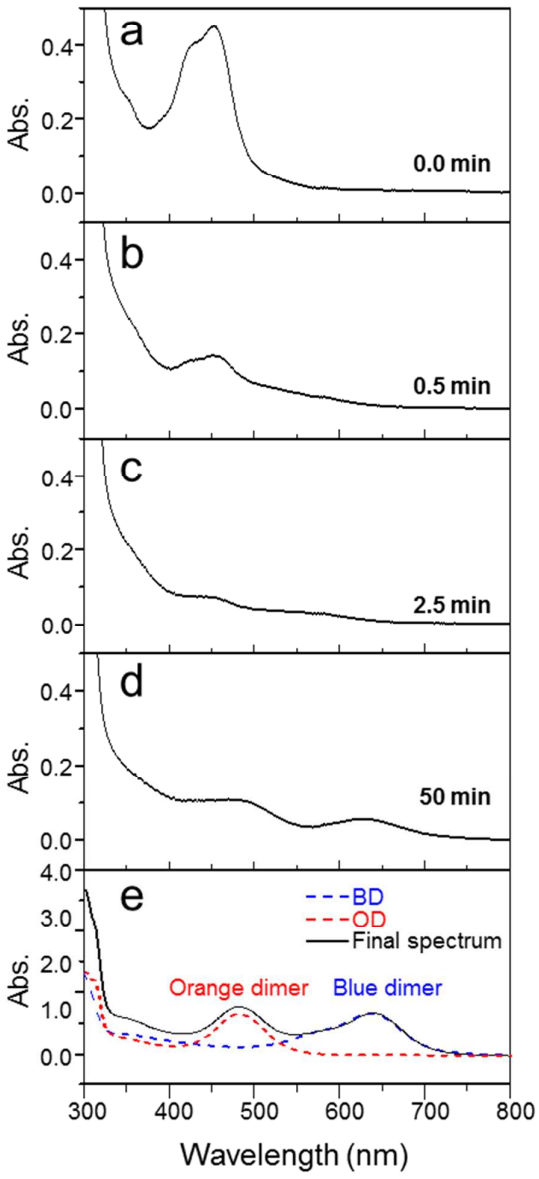

Figure 4. (a-d) The progressive spectral change of the solution consisting of $Ru(bpy)_3^{2+}$ (0.3 mM) in the presence of $S_2O_8^{2-}$ (6 mM) upon irradiation with a solar simulated light: a; 0, b; 0.5, c; 2.5, d; 50 min. (e) The comparison of the spectrum in d with those of orange and blue dimers.

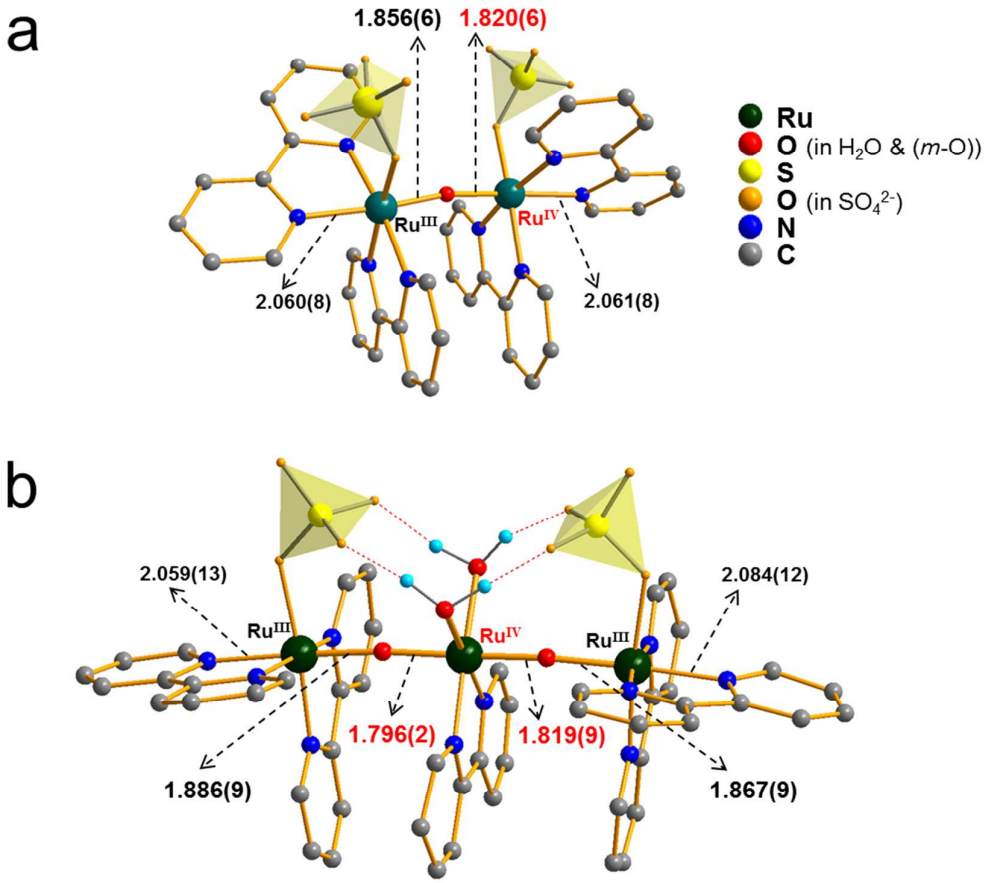

Figure 5. Crystal structures of (a) $\{[Ru^{III}(SO_4)(bpy)_2](\mu\text{-}O)[Ru^{IV}(SO_4)(bpy)_2]\}^+$ (an orange dimer analog, CCDC-**1476029**) and (b) $\{[Ru^{III}(SO_4)(bpy)_2(\mu\text{-}O)]_2Ru^{IV}(bpy)(H_2O)_2\}^{2+}$ (CCDC-**1476031).** Hydrogen atoms have been omitted for clarity in bipyridine ligands. Sulfate ions are drawn to represent the polyhedral shapes.

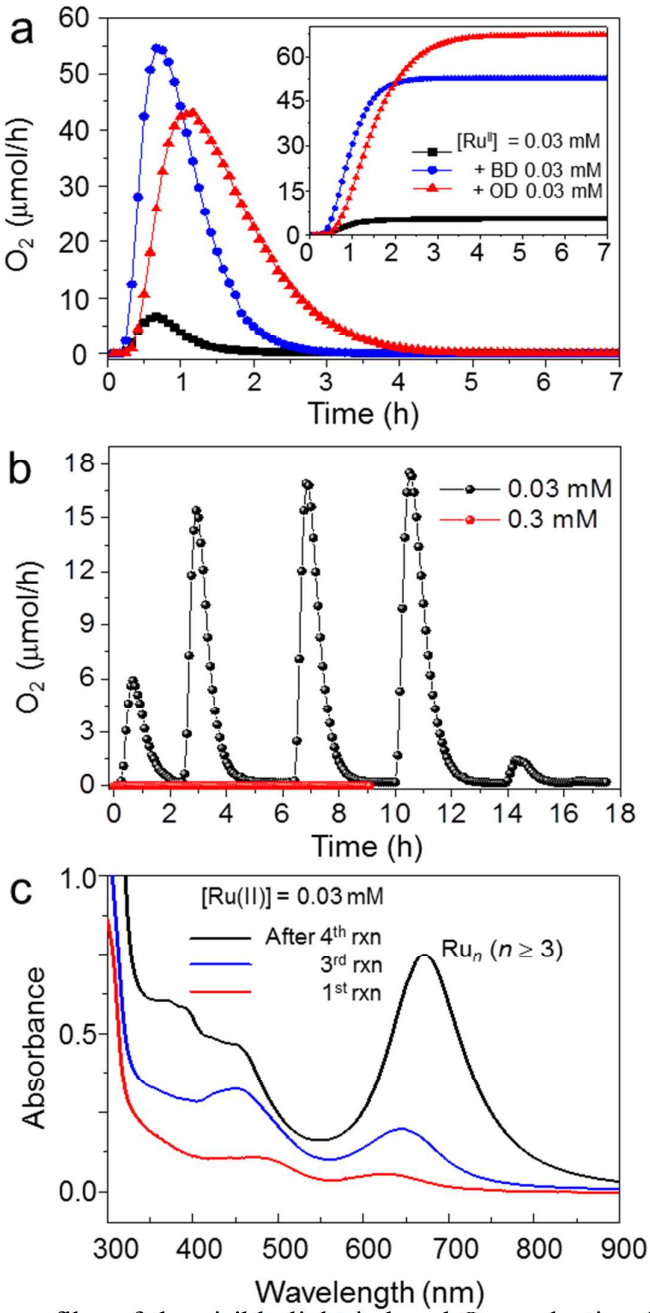

Figure 6. (a) The profiles of the visible light induced O_2 production from $Ru(bpy)_3^{2+}$ (0.03 mM) and $S_2O_8^{2-}$ (6 mM) in the presence of blue dimer (blue), orange dimer (red), and none (black). (b) The profiles of the visible light-induced O_2 production by adding fresh $Ru(bpy)_3^{2+}$ into the reaction mixture consisting of $Ru(bpy)_3^{2+}$ and $S_2O_8^{2-}$ (6 mM) after the previous reaction was finished for two different amounts of $Ru(bpy)_3^{2+}$ which corresponds to 0.03 (black) and 0.3 mM (red). (c) The progressive UV-vis spectral change of the solution on going from 1st run (red) to third run (blue), and to fourth run (black) from panel b.

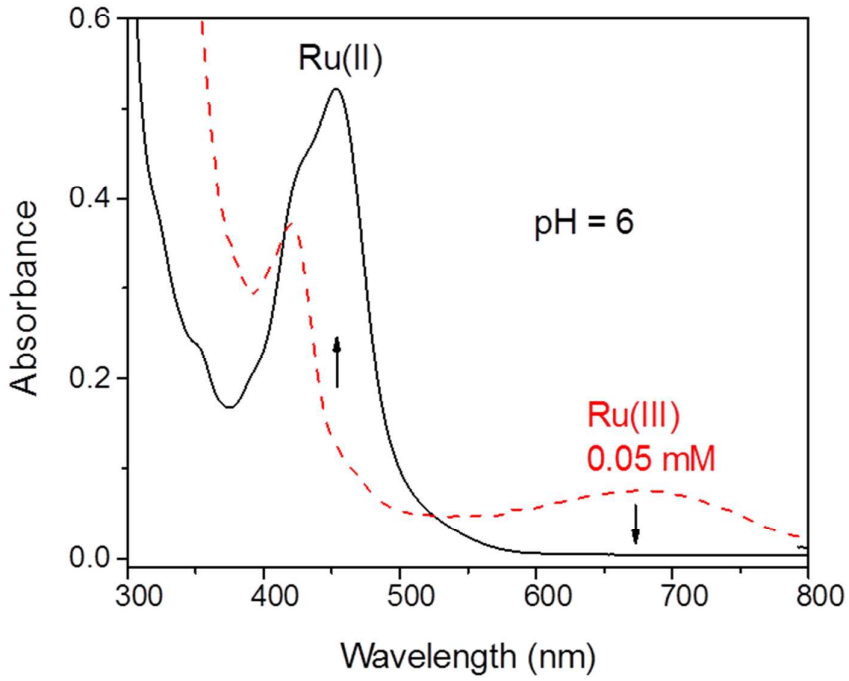

Figure 7. The full transformation of $Ru(bpy)_3^{3+}$ (0.05 mM) to $Ru(bpy)_3^{2+}$ (0.05 mM) at pH = 6.

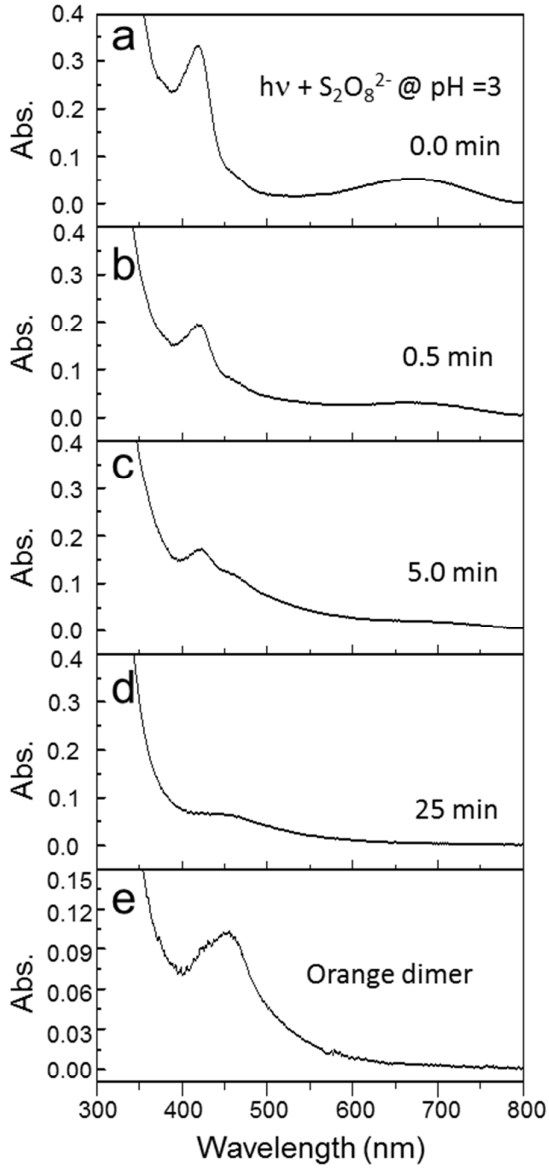

Figure 8. (a-d) The progressive spectral change of the solution consisting of $Ru(bpy)_3^{3+}$ (0.05 mM) in the presence of $S_2O_8^{2-}$ (0.6 mM) upon irradiation with a solar simulated light at pH = 3: a; 0, b; 0.5, c; 5, d; 25 min. (e) The UV-vis spectrum of orange dimer.

TOC

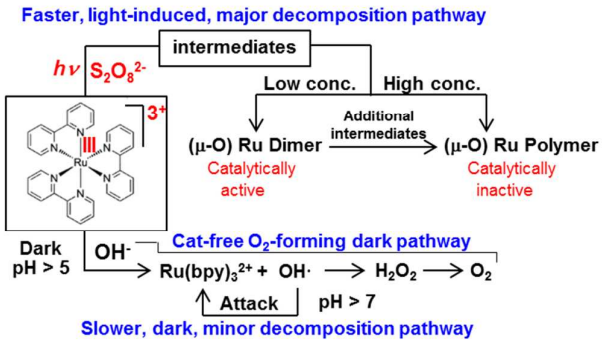
Faster, light-induced, major decomposition pathway
intermediates
hν
S2O8 2-
Low conc.
High conc.
3+
III
Ru
Additional intermediates
(μ-O) Ru Dimer
Catalytically active
(μ-O) Ru Polymer
Catalytically inactive
Dark
pH > 5
OH-
Cat-free O2-forming dark pathway
Ru(bpy)3 2+ + OH· → H2O2 → O2
Attack
pH > 7
Slower, dark, minor decomposition pathway